Electrochemical Behavior and Voltammetric Determination of a Manganese(II) Complex at a Carbon Paste Electrode

Sophia Karastogianni and Stella Girousi

Department of Analytical Chemistry, Aristotle University of Thessaloniki, Panepistimioupoli, Thessaloniki, Greece.

ABSTRACT: Investigation of the electrochemical behavior using cyclic voltammetry and detection of [Mn^{2+}(thiophenyl-2-carboxylic acid)$_2$ (triethanolamine)] with adsorptive stripping differential pulse voltammetry. The electrochemical behavior of a manganese(II) complex [Mn^{2+}(thiophenyl-2-carboxylic acid)$_2$(triethanolamine)] (**A**) was investigated using cyclic and differential pulse voltammetry in an acetate buffer of pH 4.6 at a carbon paste electrode. Further, an oxidation–reduction mechanism was proposed. Meanwhile, an adsorptive stripping differential pulse voltammetric method was developed for the determination of manganese(II) complex.

KEYWORDS: Mn(II) complex, cyclic voltammetry, differential pulse voltammetry, carbon paste electrode

CITATION: Karastogianni and Girousi. Electrochemical Behavior and Voltammetric Determination of a Manganese(II) Complex at a Carbon Paste Electrode. *Analytical Chemistry Insights* 2016:11 1–11 doi:10.4137/ACI.S32150.

TYPE: Original Research

RECEIVED: September 7, 2015. **RESUBMITTED:** November 1, 2015. **ACCEPTED FOR PUBLICATION:** November 5, 2015.

ACADEMIC EDITOR: Gabor Patonay, Editor in Chief

PEER REVIEW: Six peer reviewers contributed to the peer review report. Reviewers' reports totaled 1155 words, excluding any confidential comments to the academic editor.

FUNDING: Authors disclose no external funding sources.

COMPETING INTERESTS: Authors disclose no potential conflicts of interest.

CORRESPONDENCE: girousi@chem.auth.gr

Paper subject to independent expert blind peer review. All editorial decisions made by independent academic editor. Upon submission manuscript was subject to anti-plagiarism scanning. Prior to publication all authors have given signed confirmation of agreement to article publication and compliance with all applicable ethical and legal requirements, including the accuracy of author and contributor information, disclosure of competing interests and funding sources, compliance with ethical requirements relating to human and animal study participants, and compliance with any copyright requirements of third parties. This journal is a member of the Committee on Publication Ethics (COPE). Provenance: the authors were invited to submit this paper.

Published by Libertas Academica. Learn more about this journal.

Introduction

Manganese is a key cofactor for a broad range of metalloenzymes, including oxidases and dehydrogenases, deoxyribonucleic acid (DNA) and ribonucleic acid (RNA) polymerases, kinases, decarboxylases, and sugar transferases.[1,2] Its compounds are important in several biological systems involving an electron transfer reaction, such as reactions involving photosystem II (PSII) and supreoxide dismutase (SOD).[3,4] A few manganese complexes have been reported to show anti-reactive oxygen species (ROS) activity,[5] while Mn(II) and Mn(III) complexes have shown promising results for DNA binding and cleavage activity.[6,7] Reported Mn-SOD enzymes have a redox potential that is between the redox potentials corresponding to the reduction and oxidation of the superoxide radical (200–450 mV vs normal hydrogen electrode [NHE]).[8] Therefore, the electrochemical properties of manganese compounds are in direct relation with some of the most significant biological procedures in nature and could be very helpful to clarify the mechanism of these procedures. Furthermore, manganese complexes could have toxic effects or therapeutical properties. This implies that it is necessary to develop sensitive, fast, cost-effective detection assays of manganese complexes.

Manganese complexes are mainly used as catalysts because they contain a central metal with variable oxidation states.[9,10] However, manganese complexes with acyclic multidentate ligands are still very limited.[9] In analytical chemistry, they have been utilized as chemical modifiers of electrode surfaces for the electrochemical determination of analytes such as NO and peroxynitrite ions.[10,11] In addition, manganese complexes have been used as hybridization indicators for determining infectious agents and for monitoring sequence-specific hybridization events.[12–14] Thiophenyl-2 saturated carboxylic acid is known for its anti-inflammatory activity and its ability to coordinate with a broad range of metallic ions and produce complexes with anti-inflammatory, SOD mimetic, and other actions.[15] Meanwhile, triethanolamine is a biologically relevant ligand with great coordinative ability and flexibility.[16] Triethanolamine is widely used in cosmetology, and it belongs to the group of tripodal ligands that have been studied for their biological application as complex models for the redoxidative reaction of metal proteins. However, only few manganese complexes containing thiophenyl-2 saturated carboxylic acid (HL) and triethanolamine (H_3tea) have been reported in the literature.[15–19]

Techniques such as cyclic voltammetry (CV) and differential pulse voltammetry (DPV) are widely used in order to understand the redox behavior of metal complexes. On the other hand, adsorptive stripping voltammetry (AdSV) is a stripping electroanalytical technique,[20] where the deposition of the analyte is accomplished by a physical or chemical interaction with the electrode surface. Once sufficient deposition of the analyte is achieved, the potential of the working electrode is swept to strip the analyte from the electrode surface, with the associated faradaic current being measured to quantitatively

determine the analyte's concentration. Only a few studies exist in the literature, where manganese/ligand systems or manganese complexes were electroanalytically investigated.[21]

Electrochemical investigation of manganese complexes, such as $[Mn^{2+}(\text{thiophenyl-2-carboxylic acid})_2(H_3\text{tea})]$, that is, $[Mn^{2+}(L)_2(H_3\text{tea})]$ (**A**), is important because they may serve in the clarification of clinical results and as models for studying their role in biological systems. Metal complexes such as (**A**) can also be used as models to establish relationships between electrochemical and pharmacological properties. They can also be used to correlate the biological action of drugs and the behavior of chemical species with biochemical significance. Thus, this study describes the electrochemical behavior of this seven-coordinate and capped prismatic manganese(II) complex using CV and DPV. Therefore, this electrochemical investigation complements the existing information about the voltammetric behavior of analogous manganese complexes. Furthermore, a mechanistic scheme of oxidation and reduction of (**A**) is proposed, which could be useful in understanding the SOD mimetic action of manganese(II) ions and its compounds. Besides, AdSV is a fast and sensitive technique and has been employed in the analytical determination of (**A**) at a carbon paste electrode (CPE).

Methods

Materials and reagents. All reagents were of analytical grade and used as received. Dimethyl sulfoxide (DMSO) was obtained from Alfa Aesar. Graphite powder (50870, p.a. purity 99.9%, and particle size <0.1 mm) was purchased from Fluka. Manganese(II) complex (Fig. 1) was prepared as previously reported.[7] Then, thiophenyl-2 carboxylic acid (HL) was dissolved in MeOH and NaOH was added. After 30 minutes of stirring, triethanolamine was added, and after 15 minutes of stirring, $MnCl_2{\cdot}4H_2O$ dissolved in methanol was also added dropwise. The pale yellow mixture was slightly heated and stirred for additional 1 hour and then concentrated to half the volume. Colorless crystals of compound were obtained by slow evaporation after 2 days.

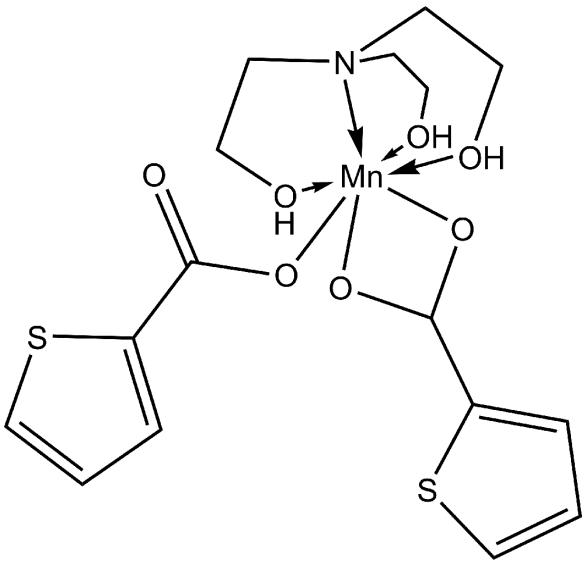

Figure 1. Chemical structure of (**A**). Solid lines correspond to the normal covalent bonds and the arrows represent the coordinate covalent bonds.

Instruments. Experiments were carried out using a μ Autolab potentiostat/galvanostat (Eco Chimie) and controlled by GPES 4.9.0005 Beta software. A platinum wire as a counter electrode and Ag/AgCl/3 mol L^{-1} KCl as a reference electrode were used. A CPE was used as a working electrode. The CPE was prepared by thoroughly mixing by hand adequate amounts of graphite powder and paraffin oil in 75/25 mass ratio. A portion of the resulting mixture was packed into the bottom of a polytetrafluoroethelene (PTFE) sleeve. The surface was manually polished to a smooth finish on a piece of weighing paper before use. All the experiments were performed at room temperature.

Stock solution preparation. Stock solutions of (**A**) were prepared in DMSO. The solutions were further diluted in the appropriate buffer as per requirement.

Procedure for the electrochemical study of (A). Suitable amounts of the stock solution of (**A**) were added to the electrochemical cell containing 0.1 mol L^{-1} acetate buffer at pH 4.6 and 0.1 mol L^{-1} KCl, and measurements were performed using CV, and DPV.

Procedure for the electrochemical detection of (A). A freshly smoothed CPE surface was immersed into 0.1 mol L^{-1} acetate buffer at pH 4.6 containing 0.02 mol L^{-1} KCl and the appropriate amount of (**A**) and conditioned at –1.5 V for anodic and +1.0 V for cathodic scan for 8 and 3 seconds, respectively. Then, a deposition potential of –1.2 V for anodic and +1.0 V for cathodic scan was applied for 90 and 180 seconds, respectively. Finally, the signal transduction was accomplished using DPV after an equilibration time of 10 seconds. The instrumental conditions for anodic scan were initial potential = +0.0 V, end potential = +1.2 V, modulation time = 0.07 second, interval time = 0.6 second, step potential = 0.003 V s^{-1}, and modulation amplitude = +0.5 V, while those for cathodic scan were initial potential = +1.0 V, end potential = +0.0 V, modulation time = 0.07 second, interval time = 1 second, step potential = 0.004 V s^{-1}, and modulation amplitude = +0.1 V. The raw data were treated using the Savitzky and Golay filter (level 2) of the GPES software, followed by the GPES software moving average baseline correction using a peak width of 0.06.

Results and Discussion

Effect of mass concentration of (A) and scan rate on CV. Figure 2 describes the effect of mass concentration of (**A**) at 1 mV s^{-1}. As shown in the figure, an anodic peak (peak 1, Fig. 2A and B) and a cathodic peak (peaks 2 and 3, Fig. 2A and B, respectively) were observed as the mass concentration of (**A**) was varied from 10 to 200 mg L^{-1}. It must be stressed that in Figure 2B, two anodic peaks (peaks 1 and 2, Fig. 2B) and a cathodic peak (peak 3, Fig. 2B) were observed, when the

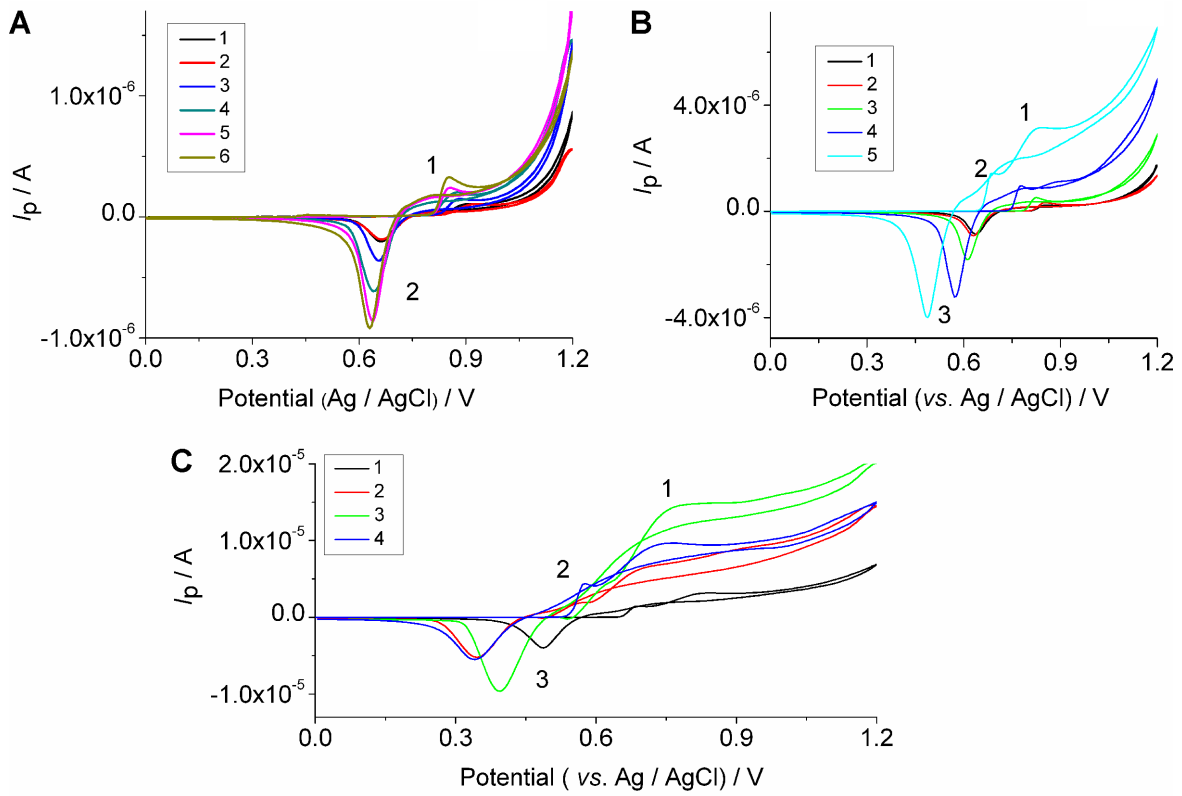

Figure 2. CVs of (**A**) (**A**) (1) 10, (2) 20, (3) 30, (4) 40, (5) 50, and (6) 80 mg L^{-1}, (**B**) (1) 50, (2) 80, (3) 100, (4) 200, and (5) 400 mg L^{-1}, and (**C**) (1) 400, (2) 600, (3) 1,000, and (4) 1,200 mg L^{-1} at 1 mV s^{-1}. (Experimental conditions as mentioned in Methods section and voltammetric conditions: start potential = first vertex potential = 0.0 mV, second vertex potential = +1,200 mV, step potential = 5 mV, and number of scans = 3).

mass concentration of (**A**) was varied from 400 to 600 mg L^{-1}. On the other hand, from 400 to 1,200 mg L^{-1} of (**A**), two anodic peaks (peaks 1 and 2, Fig. 2C) and a cathodic peak (peak 3, Fig. 2C) were observed. The peak potential of the anodic peaks (peaks 1 and 2, Fig. 2) shifted negatively as the mass concentration of (**A**) was increased. It must be noted that the cathodic peak potential (peaks 2 and 3, Fig. 2) moved to more negative values up to 1,000 mg L^{-1} of (**A**), after which the values shifted positively (peak 3, Fig. 2C). The peak potentials of oxidation and reduction peaks at different mass concentrations of (**A**) are given in Table 1.

Further, Figure 3 illustrates the typical cyclic voltammograms obtained for different mass concentrations of (**A**) at 10 mV s^{-1}. As shown in the figure, an anodic peak (peak 1, Fig. 3A) was present as the mass concentration of (**A**) ranged from 40 to 400 mg L^{-1}. In addition, a cathodic peak (peak 2, Fig. 3A) was observed when the mass concentration of (**A**) ranged from 30 to 400 mg L^{-1}. The peak potential of the anodic peak (peak 1, Fig. 3A) was moved toward more negative values as the mass concentration of (**A**) varied from 40 to 400 mg L^{-1}, while the peak potential of the cathodic peak (peak 2, Fig. 3A) shifted negatively as the mass concentration of (**A**) was increased from 30 to 400 mg L^{-1}. On the other hand, in Figure 3B, two anodic peaks (peaks 1 and 2, Fig. 3B) were obvious, when the mass concentration of (**A**) ranged from 600 to 1,200 mg L^{-1}. It is interesting to note that at 800 mg L^{-1} of (**A**), only one oxidation peak was present (peak 2, Fig. 3B). A cathodic peak was also observed in Figure 3B, when the mass concentration of (**A**) ranged from 600 to 1,200 mg L^{-1}. The peak potential of the anodic peaks 1 and 2 (Fig. 3B) shifted positively up to 1,000 mg L^{-1}, after which the values moved to more negative values. The peak potential of cathodic peak 3 (Fig. 3B) shifted negatively from 600 to 800 mg L^{-1} and positively from 800 to 1,200 mg L^{-1}. The peak potentials of oxidation and reduction peaks at different mass concentrations of (**A**) are given in Table 1.

The cyclic voltammograms of varying mass concentrations of (**A**) at 100 mV s^{-1} are depicted in Figure 4. As shown in the figure, an anodic peak (peak 1, Fig. 4A) was observed as the mass concentration of (**A**) ranged from 100 to 400 mg L^{-1}, while a cathodic peak (peak 2, Fig. 4A) was present when the mass concentration of (**A**) ranged from 10 to 400 mg L^{-1}. The peak potential of the anodic peak (peak 1, Fig. 4A) shifted positively from 10 to 20 mg L^{-1}. When the mass concentration of (**A**) varied from 20 to 80 mg L^{-1}, the cathodic peak potential of peak 2 (Fig. 4A) shifted negatively, while it remained almost constant from 80 to 200 mg L^{-1} (Fig. 4A). Above 200 mg L^{-1}, the cathodic peak potential moved to more positive values (Fig. 4A). On the other hand, in Figure 4B, one anodic peak (peak 2, Fig. 4B) was obvious, when the mass concentration of (**A**) was equal to 600 mg L^{-1}. Two anodic peaks were observed at 800 mg L^{-1} (peaks 1

Table 1. Electron transfer coefficients (αn) and standard rate constants (k_s) of (**A**) at different mass concentrations of (**A**).

γ_a/mg L^{-1}	E_p/V						αn			k_s/S^{-1}		
	ANODIC PEAK 1			ANODIC PEAK 2			CATHODIC PEAK			ANODIC PEAK 1	ANODIC PEAK 2	CATHODIC PEAK
	1 mV s^{-1}	10 mV s^{-1}	100 mV s^{-1}	1 mV s^{-1}	10 mV s^{-1}	100 mV s^{-1}	1 mV s^{-1}	10 mV s^{-1}	100 mV s^{-1}			
10	0.927	–	–	–	–	–	0.667	–	0.713	0.74	–	0.85	0.034	–	0.03
20	0.928	–	–	–	–	–	0.669	–	0.616	0.78	–	0.85	0.032	–	0.03
30	0.889	–	–	–	–	–	0.654	0.664	0.708	0.48	–	1.10	0.052	–	0.023
40	0.874	–	–	–	–	–	0.640	0.654	0.693	0.47	–	0.99	0.059	–	0.026
80	0.854	0.928	–	–	–	–	0.625	0.635	0.641	0.50	–	1.18	0.051	–	0.021
100	0.830	0.903	1.001	–	–	–	0.615	0.630	0.644	0.48	–	1.34	0.051	–	0.019
200	0.854	0.850	0.991	–	–	–	0.566	0.591	0.649	0.50	0.33	1.41	0.051	0.236	0.018
400	0.825	0.781	0.967	0.684	–	–	0.483	0.503	0.605	0.19	0.25	1.02	0.134	0.238	0.025
600	0.713	0.762		0.615	0.547	0.767	0.352	0.347	0.376	0.19	0.29	1.10	0.235	0.233	0.023
800	–	–	0.942	–	0.689	0.649	–	0.117	0.254	0.28	0.21	–	0.118	0.256	0.023
1000	0.767	0.845	–	0.605	0.606	0.771	0.391	0.410	0.410	0.29	0.27	1.29	0.115	0.241	0.020
1200	0.727	0.830	0.883	0.571	0.586	0.644	0.342	0.327	0.420	0.17	0.26	0.62	0.118	0.234	0.040

and 2, Fig. 4B). At 1,000 mg L^{-1} also, one anodic peak was found (peak 2, Fig. 4B), while at 1,200 mg L^{-1}, two anodic peaks appeared again (peaks 1 and 2, Fig. 4B). Furthermore, a cathodic peak was observed in Figure 4B, when the mass concentration of (**A**) ranged from 400 to 1,200 mg L^{-1}. The peak potential of the anodic peak 1 (peak 1, Fig. 4B) shifted negatively in the entire range of mass concentration of (**A**). Further, the peak potential of anodic peak 2 (peak 2, Fig. 4B) moved negatively from 600 to 800 mg L^{-1} and positively from 800 to 1,000 mg L^{-1}. At higher mass concentration values, the peak potential of anodic peak 2 (Fig. 4B) moved to more negative values again. The cathodic peak potential moved negatively from 400 to 800 mg L^{-1} and positively from 800 to 1,000 mg L^{-1} (Fig. 4B). Above 1,000 mg L^{-1}, the cathodic peak potential moved to more negative values.

In addition, the absence of a second cathodic peak on the cyclic voltmmograms (Figs. 2–4) indicates the presence of at least one chemical reaction step in the electrochemical procedure. The anodic and cathodic peak current heights were different, which is typical of a nonreversible electrochemical reaction. A crossover appeared, which is typical of the formation of a new phase involving a nucleation process and growth (Figs. 2A and B, 3A, and 4A).[22,23] The anodic peak current increased as the mass concentration of (**A**) was increased up to 1,000 mg L^{-1} at 1 and 10 mV s^{-1} (Figs. 2 and 3). The anodic peak 1 (Figs. 2 and 3) became rounder as the scan rate was raised from 1 to 10 mV s^{-1}.

It was mentioned that when the mass concentration of (**A**) was higher than 600 mg L^{-1} and at scan rates 10 and 100 mV s^{-1}, two anodic peaks (peaks 1 and 2, Figs. 2B and C, 3B, and 4B) and one cathodic peak (peak 3, Figs. 2B and C, 3B, and 4B) appeared in the cyclic voltammograms at the entire range of the studied scan rates. It must be stressed that at a scan rate of 1 mV s^{-1}, two anodic peaks were observed when the mass concentration of (**A**) was higher than 400 mg L^{-1} (Fig. 2B and C). This means that the oxidation of (**A**) occurred in two steps. Therefore, (**A**) is oxidized to a Mn^{3+} compound (peak 2 in Figs. 2–4), and some of the active electrode surface may still be active for the oxidation of the central ion Mn^{2+} to Mn^{3+} (peak 1 in Figs. 2–4).[21,24–30]

At 100 mV s^{-1}, the peak current height of peak 1 (Fig. 4A) was increased up to 100 mg L^{-1}. At further incensement of the mass concentration of (**A**), peak 1 (Fig. 4A) became less pronounced and peak 2 (Fig. 4B) appeared at a mass concentration higher than 600 mg L^{-1}. These observations may be explained by the less time required for the chemical reaction to occur, producing an insulating intermediate or the steric effect of the ligands that deactivate the electrode again.[22,31,32]

The reduction peak became rounder when the scan rate and mass concentration were increased (Figs. 2–4). The intensity of the peak current increased at all of the studied scan rates (Figs. 2–4). This means that the reduction of the oxidized product of (**A**), most probably, to a Mn^{2+} compound proceeded through a Mn^{3+} intermediate. These observations also indicate that the chemical reaction proceeded simultaneously.[29]

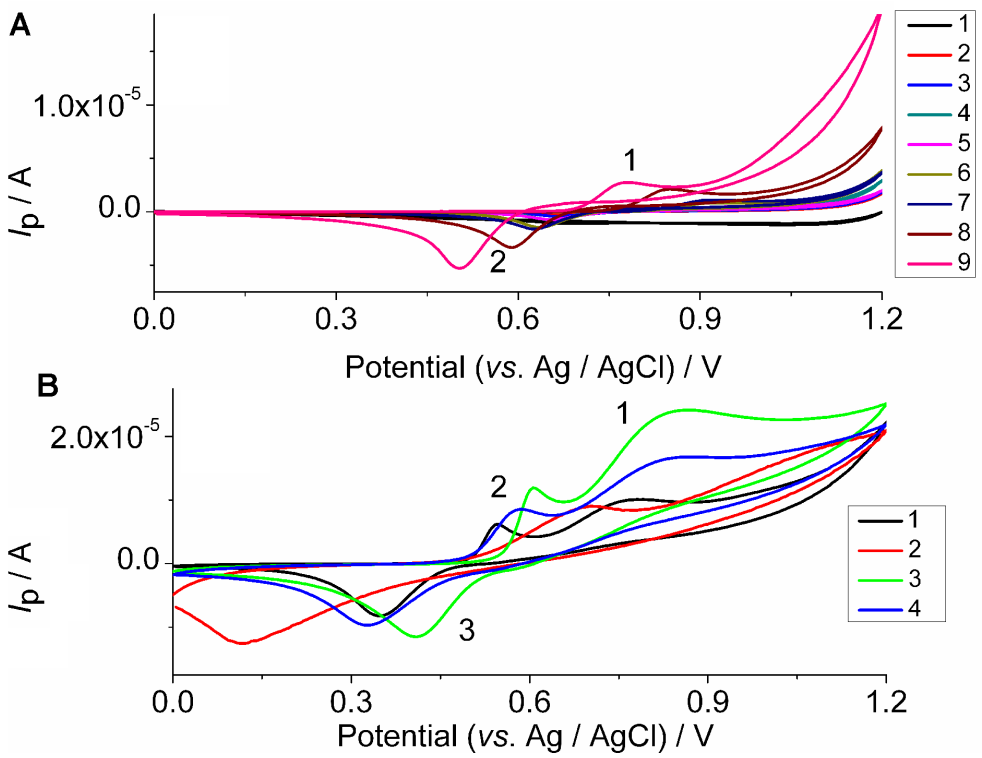

Figure 3. CVs of (**A**) in 0.1 mol L^{-1} acetate buffer at pH 4.6 containing 0.01 KCl mol L^{-1}. (**A**) (1) 10, (2) 20, (3) 30, (4) 40, (5) 50, (6) 80, (7) 100, (8) 200, and (9) 400 mg L^{-1} and (**B**) (1) 600, (2) 800, (3) 1,000, and (4) 1,200 mg L^{-1} at 10 mV s^{-1}. (Experimental and voltammetric conditions as described in Fig. 2).

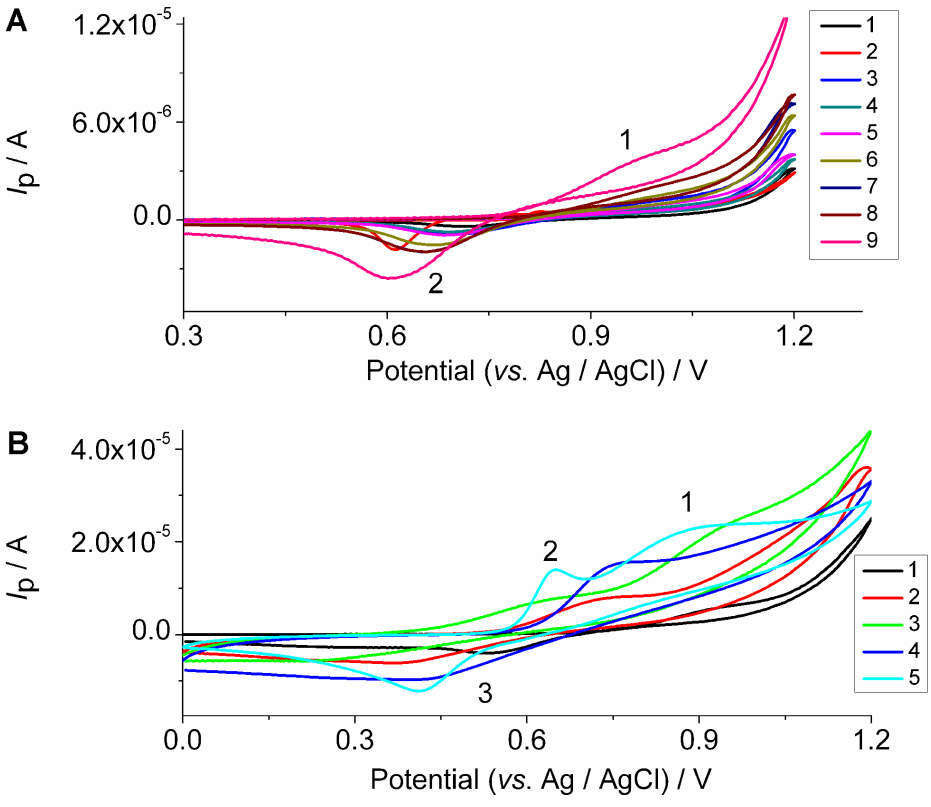

Figure 4. CVs of (**A**) in 0.1 mol L^{-1} acetate buffer at pH 4.6 containing 0.01 KCl mol L^{-1}. (**A**) (1) 10, (2) 20, (3) 30, (4) 40, (5) 50, (6) 80, (7) 100, (8) 200, and (9) 400 mg L^{-1} and (**B**) (1) 400, (2) 600, (3) 800, (4) 1,000, and (5) 1,200 mg L^{-1} at 100 mV s^{-1}. (Experimental and voltammetric conditions as described in Fig. 2).

The overpotential for the reduction of Mn^{3+} species to Mn^{2+} species decreased, owing to the larger quantities of Mn^{3+} species that are formed and the steric effect of the ligands that deactivated the CPE's surface.[22] It was found that from 10 to 40 mg L^{-1}, the anodic current of peak 1 decreased linearly with the square root of the scan rate (data are not shown), suggesting that the oxidation was diffusion controlled. From 200 to 1,200 mg L^{-1}, the anodic current of peak 2 was linearly increased with the square root of the scan rate from 1 to 20 mV s^{-1}, while for higher scan rates, it was linearly decreased, which is also indicative of a diffusion-controlled process (data are not shown). The cathodic peak current was linearly decreased with the square root of the scan rate from 50 to 600 mg L^{-1}, which is indicative of quasireversible reactions, while for higher mass concentrations, it linearly increased (data are not shown).

The current of peak 1 was linearly decreased with the scan rate of up to 1,000 mg L^{-1}, when the scan rate was raised from 1 to 20 mV s^{-1}, while for higher scan rates, the dependence was not linear (data are not shown). The current of peak 2 was linearly increased with the scan rate from 1 to 20 mV s^{-1}, but for higher scan rates, it linearly decreased (data are not shown). The cathodic peak current linearly increased from 50 to 600 mg L^{-1} and then linearly decreased when the scan rate was increased (data are not shown). These facts are indicative of adsorption.[32]

The peak potential of all the peaks was directly proportional to the logarithm of scan rate in all of the studied mass concentrations (data are not shown). From the slope of this diagram, the electron transfer coefficient was calculated (Table 1). Generally, the electron transfer coefficient of anodic peaks 1 and 2 was decreased as the mass concentration of (**A**) was increased. On the other hand, it increased with increasing the mass concentration of (**A**) up to its maximum value at 200 mg L^{-1} and then decreased for the cathodic peak.

It was found that the current function $I_p/\gamma v^{1/2}$ of all peaks decreased, when the scan rate was increased in the studied range of mass concentration (data are not shown), which is a further indication of the participation of adsorption in the oxidation and reduction.[33] Moreover, the linear shape of I_p/γ vs γ graph of all peaks at low mass concentrations is consistent with the presence of adsorption in the oxidation and reduction (data are not shown).[33]

The Laviron's equation was used to estimate the standard rate constant (k_s) values (Table 1).[34] From Table 1, it is obvious that k_s was increased up to 600 mg L^{-1} for anodic peak 1, after which it decreased, while for anodic peak 2 and cathodic peak, it remained almost constant. Generally, large values of k_s indicate the high ability of (**A**) for promoting electron transfer at the electrode surface. This ability is higher for oxidation peaks and increased as the mass concentration of (**A**) was increased.

Effect of the buffer pH on CV. Two levels of mass concentration of (**A**) were investigated, ie, 50 and 600 mg L^{-1}. There was an absence of peaks at both mass concentrations when the pH was lower than 3.8, probably due to the production of a compound with Mn^{3+} species or to the incomplete precipitation of MnO_2.[24] These species are unstable in acidic media and could be reduced to Mn^{2+} species. Therefore, oxidation and reduction peak currents were largely reduced.

One anodic and a cathodic (Fig. 5A) peak appeared at 50 mg L^{-1}, when the pH ranged from 3.8 to 5.8. At pH 5.6 and 5.8, the anodic peak split into two peaks, when the mass concentration was 50 mg L^{-1} (Fig. 5A). This split could be related to the adsorption of the oxidized (**A**) on CPE and even to traces of water content.[31] Two anodic peaks (Fig. 5B) were observed at 600 mg L^{-1} at the same pH range.

The anodic peak at 50 mg L^{-1} and the second anodic peak at 600 mg L^{-1} could be assigned to the oxidation of (**A**) to a Mn^{4+} compound.[21,24–30] The first anodic peak at 600 mg L^{-1} could correspond to the oxidation of (**A**) to a Mn^{3+} compound.[21,24–30] Moreover, the cathodic peak (Fig. 5A and B) at both mass concentrations could be attributed to the reduction of Mn^{4+} compound to a Mn^{2+} compound through a Mn^{3+} intermediate.[21,24–30] It must be stressed that H_3tea (at low mass concentration) and HL were inactive.[35,36]

At 600 mg L^{-1}, one anodic peak (Fig. 5C) was evident, when the pH ranged from 6.0 to 10.0. The magnitude of this peak potential was close to that of H_3tea.[35] At pH higher than 10.0 at both mass concentrations, the decrease in the oxidation and reduction peak current, as well as the brown color of the solution, was probably due to the increasingly competitive production of $Mn(OH)_4$.

The peak potential of anodic and cathodic peaks was found to be linearly proportional to pH at both mass concentrations. At 50 mg L^{-1}, the obtained slope for the oxidation peak was calculated to be –184.6 ± 2.01 mV/pH, which is close to the theoretically predicted value from the Nernst equation (177.5 mV/pH) for a six-proton and two-electron reaction. At 600 mg L^{-1}, the slopes obtained for the first and second anodic peaks were found to be –175.6 ± 2.13 mV/pH and –177.6 ± 3.61 mV/pH, respectively, which are close to the theoretical value (177.5 mV/pH) for a three-proton and one-electron reaction. The experimental values of the slope at 50 and 600 mg L^{-1} for the reduction peak were found to be –116.4 ± 0.89 mV/pH and –112.3 ± 2.26 mV/pH, respectively. These values are close to the theoretical value (118.4 mV/pH) for a four-proton and two-electron reaction. In the case of the oxidation peak at pH values higher than 6.0, the slope was calculated to be equal to 26.80 ± 1.42 mV/pH, which is favorably close to that of H_3tea.[35]

Proposed oxidation–reduction mechanism. The following electron electron chemical (EEC) mechanism is envisaged for the anodic deposition of (**A**)[26]: First, (**A**) is diffused from the bulk solution to the CPE's surface according to Equation 1.

$$[Mn^{2+}(L)_2(H_3tea)]_{sol} \rightarrow [Mn^{2+}(L)_2(H_3tea)]_{surf}, \quad (1)$$

Subsequently, at lower concentration of (**A**), the $[Mn^{2+}(L)_2(H_3tea)]_{surf}$ is oxidized according to Equation 2, Figures 2A and B, 3A, and 4A.[26]

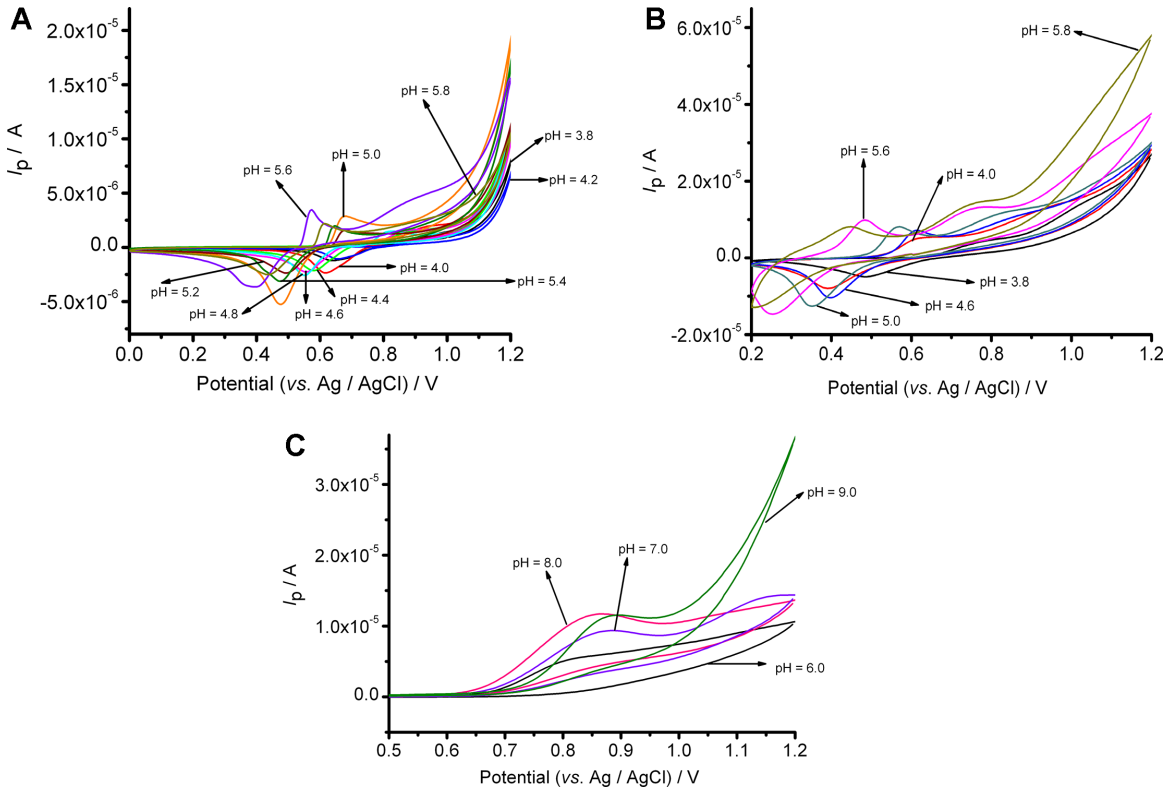

Figure 5. CVs of (**A**) at various pH values: (**A**) 50 mg L^{-1} of (**A**) at pH range from 3.8 to 5.8, (**B**) 600 mg L^{-1} of (**A**) at pH range from 3.8 to 5.8, and (**C**) 600 mg L^{-1} of (**A**) at pH range from 6.0 to 9.0. (Voltammetric conditions: step potential = 5 mV, scan rate = 25 mV s^{-1}, and number of scans = 3).

$$[Mn^{2+}(L)_2(H_3tea)]_{surf} \rightarrow [Mn^{3+}(L)_2(H_3tea)]^+_{ads} + e^-, \quad (2)$$

The oxidation of $[Mn^{2+}(L)_2(H_3tea)]_{surf}$ to $[Mn^{4+}(L)_2(Htea)]_{ads}$ suggests the simultaneous oxidation of a water molecule, as shown by Equation 3.[26]

$$H_2O \rightarrow OH_{ads} + H^+ + e^-, \quad (3)$$

On the other hand, the $[Mn^{3+}(L)_2(H_3tea)]^+_{ads}$ is dissociated according to Equation 4.[26]

$$2[Mn^{3+}(L)_2(H_3tea)]^+_{ads} \rightarrow [Mn^{2+}(L)_2(H_3tea)]_{ads} + [Mn^{4+}(L)_2(Htea)]_{ads} + 2H^+, \quad (4)$$

The produced above mentioned adsorbed on CPE's surface hydroxyl radical (Equation 3) was subsequently reacted with $[Mn^{2+}(L)_2(H_3tea)]_{ads}$ (Equation 4) and formed $[Mn^{4+}O_2(L)_2(Htea)]^{4-}_{ads}$ on CPE's surface according to Equation 5 (peaks 1, 2 and 3 in Fig. 2A and B and peaks 1 and 2 in Fig. 4A) .[26]

$$[Mn^{2+}(L)_2(H_3tea)]_{ads} + 2OH_{ads} \rightarrow [Mn^{4+}O_2(L_2(Htea)]^{4-}_{ads} + 4H^+, \quad (5)$$

Meanwhile, $[Mn^{4+}(L)_2(Htea)]_{ads}$ is hydrolyzed according to Equation 6, Figures 2A and B, 3A, and 4A.[26]

$$[Mn^{4+}(L)_2(Htea)]_{ads} + 2H_2O \rightarrow [Mn^{4+}O_2(L)_2(Htea)]^{4-}_{ads} + 4H^+, \quad (6)$$

Alternatively, the oxidation of (**A**) could also follow Equations 1 and 2, but $[Mn^{3+}(L)_2(H_3tea)]^+_{ads}$ could be hydrolyzed, and thus the oxidation could be proceeded accordingly to the following ECE mechanism (Equations 7 and 8), Figures 2A and B, 3A, and 4A[22,28,29]:

$$[Mn^{3+}(L)_2(H_3tea)]^+_{ads} + 2H_2O \rightarrow [Mn^{3+}OOH(L)_2(H_3tea)]^{2-}_{ads} + 3H^+, \quad (7)$$

$$[Mn^{3+}OOH(L)_2(H_3tea)]^{2-}_{ads} \rightarrow [Mn^{4+}O_2(L)_2(Htea)]^{4-}_{ads} + 3H^+ + e^-, \quad (8)$$

Nucleation of $[Mn^{4+}O_2(L)_2(Htea)]^{4-}$ at low scan rates and mass concentrations is due to the presence of the MnO_2 unity and is dominated by an equilibrium involving a Mn^{3+} intermediate, Equations 4 and 7 (Figs. 2A and B and 3A).[22] Subsequent growth of $[Mn^{4+}O_2(L)_2(Htea)]^{4-}$ involves the reduction of $[Mn^{4+}O_2(L)_2(Htea)]^{4-}$ surfaces by $[Mn^{2+}(L)_2(H_3tea)]$ in solution to form $[Mn^{4+}(L)_2(Htea)]$ and/or $[Mn^{3+}OOH(L)_2(H_3tea)]^{2-}$ (Equation 9 and 10), depending on the local pH and potential (Figs. 2A and B and 3A)[23]:

$$[Mn^{2+}(L)_2(H_3tea)] + [Mn^{4+}O_2(L)_2(Htea)]^{4-} + 3H^+ \rightarrow [Mn^{3+}OOH(L)_2(H_3tea)]^{2-} + [Mn^{3+}(L)_2(H_3tea)]^+, \quad (9)$$

$$[Mn^{2+}(L)_2(H_3tea)] + [Mn^{4+}O_2(L)_2(Htea)^{4-} + 2H_2O \rightarrow 2[Mn^{3+}OOH(L)_2(H_3tea)]^{2-}, \quad (10)$$

This means that at low mass concentrations, the diffusion of (**A**) from bulk solution to the $[Mn^{4+}O_2(L)_2(Htea)]^{4-}$/electrolyte interface is a factor controlling the growth of $[Mn^{4+}O_2(L)_2(Htea)]^{4-}$ and it follows a CE mechanism, in which the chemical step is rate determining.[22,23]

At high mass concentration (Figs. 2C, 3B, and 4B), it is more likely that the oxidation proceeded according to Equations 1, 2, 7, and 8 because protons and electrons that participated to these equations fulfill the experimental ones. Thus, the first oxidation peak is attributed to Equations 1, 2, and 7 and the second oxidation peak to Equation 8 (Figs. 2C, 3B, and 4B). At low scan rates, the nucleation of $[Mn^{4+}\ O_2(L)_2(Htea)]^{4-}$ also took place according to Equations 9 and 10 (Fig. 2C).

The reverse process in scanning the potential in a negative direction is ECE mechanism (Equations 11–13) (Figs. 2–4), assuming perfect stoichiometry of the MnO_2 unity:

$$[Mn^{4+}O_2(L)_2(Htea)]^{4-}_{ads} + H^+ + e^- \rightarrow [Mn^{3+}OOH(L)_2(Htea)]^{4-}_{ads}, \quad (11)$$

$$[Mn^{3+}OOH(L)_2(Htea)]^{4-}_{ads} + 3H^+ \rightarrow [Mn^{3+}(L)_2(Htea)]^-_{ads} + 2H_2O, \quad (12)$$

$$[Mn^{3+}(L)_2(Htea)]^-_{ads} + e^- \rightarrow [Mn^{2+}(L)_2(Htea)]^{2-}_{ads}, \quad (13)$$

In fact, there are several different crystalline forms of the MnO_2 unity, which could influence the ease of reductive dissolution.[26,29,30,37] In addition, $[Mn^{4+}\ O_2(L)_2(Htea)]^{4-}$ could be hydrolyzed according to Equation 14.

$$2[Mn^{4+}O_2(L)_2(Htea)]^{4-} + 2H_2O + 8H^+ \rightarrow MnO_2 + Mn(OH)_4 + 4HL + 2H_3tea, \quad (14)$$

Electrochemical detection of (A). Figure 6 shows the differential pulse voltammograms that correspond to the oxidation of (**A**) at different mass concentrations of (**A**). The oxidation signal 1 (Fig. 6) refers to the oxidation of accumulated (**A**) to $[Mn^{3+}(L)_2(H_3tea)]+$, while oxidation signal 2 (Fig. 6) is ascribed to $[Mn^{4+}\ O_2(L)_2(Htea)]^{4-}$. On the other hand, signal 3 (Fig. 6) corresponds to the oxidation of H_3tea. It should be stressed that peak 3 (Fig. 6) appeared in a narrow range of mass concentration of (**A**), and thus the subsequent investigation was focused on peaks 1 and 2 (Fig. 6).

Figure 7 shows the differential pulse voltammograms that correspond to the reduction of (**A**) at different mass concentrations of (**A**). The reduction signal refers to the reduction of accumulated $[Mn^{4+}\ O_2(L)_2(Htea)]^{4-}$ to $[Mn^{2+}(L)_2(Htea)]^{2-}$ (Fig. 7).

Calibration curves (inset of Figs. 6 and 7) were plotted under selected conditions (Table 2), and the analytical features are given in Table 2. The limits of detection and limits of quantification were calculated to be $3 \times s_b/a$ and $10 \times s_b/a$, respectively, where s_b and a are the standard deviation of the intercept and the slope of the calibration plot, respectively.[38] Thus, the results of the proposed electrochemical determination assay of (**A**) have shown promising results for the indirect Mn detection in real samples.

There is always the possibility of interference of other ionic metallic species to the detection of (**A**) and therefore

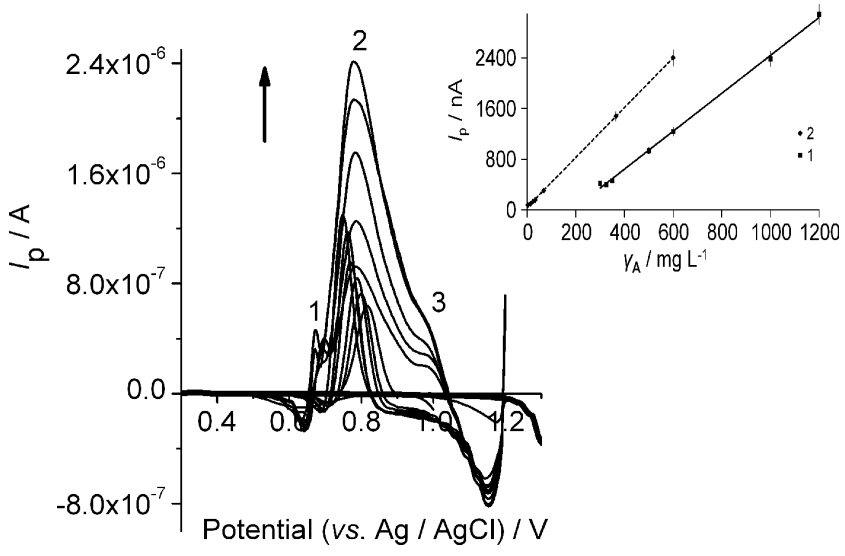

Figure 6. DPVs under selected conditions at different mass concentrations of (**A**). Inset related calibration graph: (1) peak at 0.880 V and (2) peak at 0.638 V (experimental conditions were as described in Methods section).

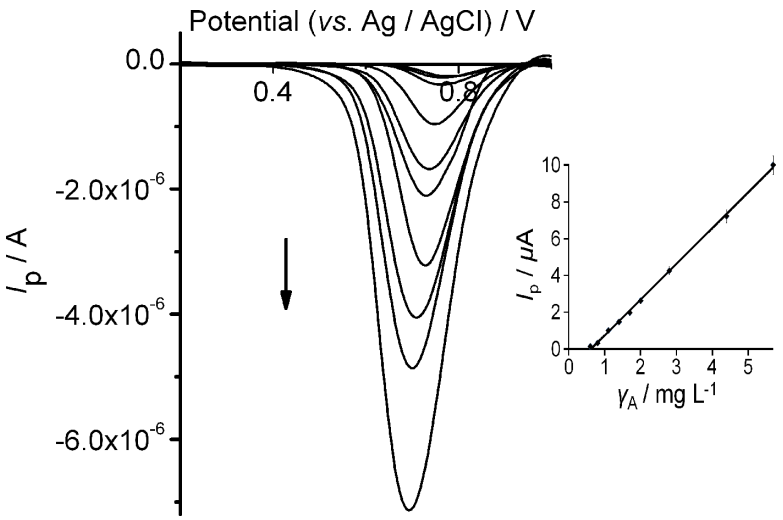

Figure 7. DPVs under selected conditions at different mass concentrations of (**A**). Inset related calibration graph of reduction peak (experimental conditions were as described in Methods section).

to the indirect detection of Mn^{2+} ions. Thus, Zn^{2+}, Cu^{2+}, Cd^{2+}, Ni^{2+}, Pb^{2+}, Fe^{3+}, Fe^{2+}, Hg^{2+}, Al^{3+}, and Cr^{+6} could be potent interferences to the proposed determination of manganese. Saterlay et al found that Zn^{2+}, Cu^{2+}, Fe^{3+}, and Pb^{2+} had no measurable effect upon response to manganese at boron-doped diamond electrode, even when present at concentrations exceeding 100-fold that of manganese.[39] They also discovered that the presence of Hg^{2+} in solution at levels at least 50-fold those of manganese also had no effect.[39] The same technique was tolerant to nearly a fivefold excess over manganese of $A1^{3+}$.[39] This group also found that the presence of Fe^{2+} in solution in amounts equal to that of manganese was sufficient to disrupt the analysis. However, this problem could be easily overcome by oxidizing Fe^{2+} to Fe^{3+} electrolytically, by driving the potential of the working electrode anodically prior to analysis.[39] The problem of Fe^{2+} interference could also be removed by complexation of Fe^{2+} ions with fluoride.[39] On the other hand, Filipe et al determined that Cd^{2+}, Cr^{6+}, and Zn^{2+} do not interfere in manganese detection at carbon film electrodes even when present in a 109-fold excess.[23] Furthermore, they found that Ni^{2+} and Cu^{2+} lower the peak height if the concentration is 109-fold excess. They also discovered that Pb^{2+} in concentrations equal to that of manganese does not interfere.[23] Finally, they also found that Fe^{2+} in equimolar amounts affects the determination of manganese ions.[23]

Conclusions

The oxidation and reduction mechanism of (**A**) was proposed based on CV data. It involves diffusion of (**A**) to the CPE's surface and its subsequent oxidation to Mn^{3+} intermediate species. It was found that at low mass concentration of (**A**), these Mn^{3+} species either dissociated disproportionately or hydrolyzed. In

Table 2. Selected conditions and detection analytical features of (**A**) using AdSV.

	OXIDATION PEAK 1	OXIDATION PEAK 2	REDUCTION PEAK
Peak potential/V	0.638	0.880	0.740
E_{cond}/V	–1.5	–1.5	–1.0
t_{cond}/s	8	8	8
E_{dep}/V	–1.2	–1.2	+1.0
t_{dep}/s	90	90	180
Regression equation	I_p (nA) = 0.00310 (±0.00001) γ_1(mg L^{-1}) – 0.61350 (±0.00798)	I_p (nA) = 0.00412 (±0.00002) γ_1 (mg L^{-1}) + 0.03788 (±0.00407)	I_p (μA) = 1.941 (±0.023) γ_1 (mg L^{-1}) – 1.196 (±0.065)
Linear range/mg L^{-1}	25.81–1200	9.885–600,0	0.333–5,700
r	0.9997	0.9998	0.9998
s_r/% (n = 6)	5.3–5,5[a]	4.0–4,2[b]	4.1–4.4[c]
LOD/mg L^{-1}	8.518	4.937	0.108
LOQ/mg L^{-1}	25.81	9.885	0.3321

Notes: Relative standard deviation at two levels of mass concentration of (**A**): [a]75.0 and 500.0 mg L^{-1}, [b]51.00 and 100.0 mg L^{-1}, and [c]0.800 and 3.67 mg L^{-1}.

the case of disproportionation of Mn^{3+} species, the products reacted with the resultant product from the oxidation of H_2O adsorbed onto the CPE hydroxide radicals, leading to the formation of an adsorbed product onto the CPE surface of Mn^{4+} compound, which bears a MnO_2 entity. On the other hand, in the case of hydrolysis of Mn^{3+} species, the products were oxidized, leading to the formation of the same adsorbed product onto the CPE Mn^{4+} compound. Two oxidation peaks were found at high mass concentration of (**A**). The first oxidation peak was also attributed to the oxidation of (**A**) to the above-mentioned Mn^{3+} intermediate species, and the second oxidation peak was ascribed to the oxidation of the hydrolysis product of the above-mentioned Mn^{3+} compound to some of the above-mentioned Mn^{4+} compounds with a MnO_2 entity. Nucleation and growth of the Mn^{4+} compound with the MnO_2 entity took place at the interface electrode surface/deposit layer. The presence of (**A**) in the electrolyte affects the reduction of the deposit Mn^{4+} compound through a chemical equilibrium. The electrochemical (CV) data gave evidence that the redox potential of (**A**) was in the proper range for a SOD biomimetic, which is a promising fact for the SOD catalytic activity of manganese complex, since optimal SOD activity in aqueous solution requires redox potentials reasonably close to +0.360 V vs NHE.[7] Based on (**A**)'s SOD activity, it could be used in the treatment of pathogenic situations where the demand for the decrease of ROS generation and oxidative stress is necessary, and thus, it could inhibit the endothelial activation. In this manner, it could also be a promising tool in antioxidant sensing.

The combination of AdSV and CPE has been shown to produce an effective and fast electroanalytical technique for the determination of (**A**) and demonstrates yet another use for this cheap and robust electrode material. Thus, the proposed electrochemical determination assay of (**A**) has shown promising results for the indirect detection of manganese in real samples in the future. Furthermore, based on the nucleation and growth properties of the resulted Mn^{4+} compound on CPE's surface, (**A**) could be used as a coating material on a chip device or as a chemical modifier of electrode surfaces to provide better detection limits to a broad range of analytes such as toxic and infectious agents. Using AdSV and CPE has also removed the problem of intermetallic species interference, which often occurs when using anodic stripping voltammetry (ASV) methodologies, allowing the use of a mercury-free working electrode and offering obvious environmental benefits.

However, the proposed methodology bears the limitations provided by the use of the CPE. This means that a well-skilled person must be employed to handle the carbon paste in order to achieve the maximum reproducibility of the fabricated electrode. Furthermore, this electrode is operative only to positive potentials. On the other hand, manganese is also a difficult metal to handle, owing to its flexible valence. In addition, the nucleation process of the MnO_2 entity of the resulted Mn^{4+} compound onto CPE proceeded slowly, suggesting the existence of an induction time for the deposition.[23] The selection of the proper potential in the preconcentration step overcomes this limitation. Finally, it is possible that some other metallic ions such as Co^{2+}, Fe^{2+}, Ni^{2+}, Zn^{2+}, or Cu^{2+} could interfere.

Author Contributions

Conceived and designed the experiments: SK. Analyzed the data: SK. Wrote the first draft of the manuscript: SK. Contributed to the writing of the manuscript: SG. Agreed with manuscript results and conclusions: SG. Jointly developed the structure and arguments for the paper: SG. Made critical revisions and approved the final version: SG. All authors reviewed and approved the final manuscript.

REFERENCES

1. Crowley JA, Traynor DA, Weatherburn DC. Manganese and its role in biological processes. In: Sigel A, Sigel H, eds. *Metal Ions in Biological Systems*. Vol 37. New York: Marcel Dekker; 1999:209–257.
2. Keen CL, Ensunsa JL, Clegg MS. Manganese and its role in biological processes. In: Sigel A, Sigel H, eds. *Metal Ions in Biological Systems*. Vol 37. New York: Marcel Dekker; 1999:90–114.
3. Umena Y, Kawakami K, Shen JR, Kamiya N. Crystal structure of oxygen evolving photosystem II at a resolution of 1.9 Å. *Nature*. 2011;473:55–60.
4. Najafpour MM, Ehrenberg T, Wiechen M, Kurz P. Calcium manganese(III) oxides ($CaMn_2O_4\ xH_2O$) as Biomimetic oxygen-evolving catalysts. *Angew Chem Int Ed*. 2010;49:2233–2237.
5. Jian G, Kai-Ju W, Jia N, Ju-Zhou Z. Hydrothermal synthesis, crystal structure, and biological properties of a Mn(II) complex with phenylformic acid-imidazole ditopic ligands. *Synth React Inorg Met Org Chem*. 2008;38:562–566.
6. Bin P, Wen-Hui Z, Lin Y, Han-We L, Li Z. DNA-binding and cleavage studies of chiral Mn(II) salen complexes. *Trans Met Chem*. 2009;34:231–237.
7. Karastogianni S, Dendrinou-Samara C, Ioannou E, Raptopoulou CP, Hadjipavlou-Litina D, Girousi S. Synthesis, characterization, DNA binding properties and antioxidant activity of a manganese(II) complex with NO_6 chromophore. *J Inorg Biochem*. 2013;118:48–58.
8. Barrette WCJ, Sawyer DT, Fee JA, Asada K. Potentiometric titrations and oxidation-reduction potentials of several iron superoxide dismutases. *Biochemistry*. 1983;22:624–627.
9. Ammam M, Keita B, Nadjo L, et al. Cyclic voltammetry study of the Mn-substituted polyoxoanions [MnII4(H2O)2(H4AsW15O56)2]18 and [(MnI-IOH2)MnII2PW9O34)2(PW6O26)]17: electrodeposition of manganese oxides electrocatalysts for dioxygen reduction. *Electroanalysis*. 2011;23:1427–1434.
10. Koca A, Özçeşmeci M, Hamuryudan E. Substituents effects to the electrochemical, and in situ spectroelectrochemical behavior of metallophthalocyanines: electrocatalytic application for hydrogen evolution reaction. *Electroanalysis*. 2010;22:1623–1633.
11. Diab N, Schuhmann W. Electropolymerized manganese porphyrin/polypyrrole films as catalytic surfaces for the oxidation of nitric oxide. *Electrochim Acta*. 2001;47:265–273.
12. Karastogianni S, Girousi S. Detection of short oligonucleotide sequences of hepatitis virus B using electrochemical DNA hybridization biosensor. *Chem Paper*. 2015;69:202–210.
13. Koh WCA, Son JI, Choe ES, Shim YB. Electrochemical detection of peroxynitrite using a biosensor based on a conducting polymer-manganese ion complex. *Anal Chem*. 2010;82:10075–10082.
14. Niu S, Zhao M, Ren R, Zhang S. Carbon nanotube-enhanced DNA biosensor for DNA hybridization detection using manganese(II)–Schiff base complex as hybridization indicator. *J Inorg Biochem*. 2009;103:43–49.
15. Pontiki E, Hadjipavlou-Litina D. Antioxidant and anti-inflammatory activity of aryl-acetic and hydroxamic acids as novel lipoxygenase inhibitors. *Med Chem*. 2006;2:251–264.
16. Topcou Y, Andac O, Yilmaz YT, Harrison WTA. () Synthesis, molecular and crystal structure of bis(triethanolamine)manganese(II) sacharinate: a seven coordinate manganese complex with tri- and tetradentate triethanolime ligands. *J Mol Struct*. 2002;610:99–103.
17. Reboucas JS, Spasojevic I, Batinic-Haberle I. Pure manganese(III) 5,10,15,20-tetrakis(4-benzoic acid)porphyrin (MnTBAP) is not a superoxide dismutase mimic in aqueous systems: a case of structure–activity relationship as a watchdog mechanism in experimental therapeutics and biology. *J Biol Inorg Chem*. 2008;13:289–302.

18. Djebbar-Sid S, Benali-Baitich O, Deloume JP. Synthesis, characterization, electrochemical and catalytic activity of manganese(II) complexes with linear and tripodal tetradentate ligands derived from Schiff bases. *Trans Met Chem*. 1998;23:443–447.
19. Paluchowska B, Maurin JK, Leciejewiz J. X-ray diffraction study on manganese(II) complexes with thiophene-2-carboxylate and furan-3-carboxylate ligands. *J Coord Chem*. 2000;51:335–347.
20. El-Maali NA, El-Hady DA. Square-wave adsorptive stripping voltammetry at glassy carbon electrode for selective determination of manganese. Application to some industrial samples. *Anal Chim Acta*. 1998;370:239–249.
21. Abollino O, Aceto M, Sarzanini C, Mentasti E. Behavior of different metal/ligand systems in adsorptive cathodic stripping voltammetry. *Electroanalysis*. 1999;11:870–878.
22. Nijjer S, Thonstad J, Haarberg GM. Oxidation of manganese(II) and reduction of manganese dioxide in sulphuric acid. *Electrochim Acta*. 2000;46:395–399.
23. Filipe OMS, Brett CMA. Cathodic stripping voltammetry of trace Mn(II) at carbon film electrodes. *Talanta*. 2003;61:643–645.
24. Paul RL, Cartwright A. The mechanism of the deposition of manganese dioxide: part III. Rotating ring-disc studies. *J Electroanal Chem Interfacial Electrochem*. 1986;201:123–131.
25. Mansouri Majd S, Teymourian H, Salimi A, Hallaj R. Fabrication of electrochemical theophylline sensor based on manganese oxide nanoparticles/ionic liquid/chitosan nanocomposite modified glassy carbon electrode. *Electrochim Acta*. 2013;108:707–716.
26. Rodrigues S, Munichandraiah N, Shukla AK. A cyclic voltammetric study of the kinetics and mechanism of electrodeposition of manganese dioxide. *J Appl Electrochem*. 1998;28:1235–1241.
27. Wu BL, Lincot D, Vedel J, Yu LT. Voltammetric and electrogravimetric study of manganese dioxide thin film electrodes. Part 1. Electrodeposited films. *J Electroanal Chem*. 1997;420:159–165.
28. Kao WH, Weibel VJ. Electrochemical oxidation of manganese(II) at a platinum electrode. Electrochemical oxidation of manganese(II) at a platinum electrode. *J Appl Electrochem*. 1992;22:21–27.
29. Petitpierre JP, Comninellis C, Plattner E. Oxydation Du MnSO4 en dioxyde de manganese dans H2SO4 30%. *Electrochim Acta*. 1990;35:281–287.
30. Bodoardo S, Brenet J, Maja M, Spinelli P. Electrochemical behavior of MnO2 electrodes in sulfuric acid. *Electrochim Acta*. 1994;39:1999–2004.
31. Budnikov GK, Troeporskaya TV. Electrochemistry of metal chelates in non-aqueous media. *Usp Khim*. 1979;48:829–853.
32. Bard AJ, Faulkner LR. *Electrochemical Methods: Fundamentals and Applications*. New York: J. Wiley & Sons; 2001.
33. Wopsschall RH, Shain I. Effects of adsorption of electroactive species in stationary electrode polarography. *Anal Chem*. 1967;39:1514–1527.
34. Laviron E. General expression of the linear potential sweep voltammogram in the case of diffusionless electrochemical systems. *J Electroanal Chem Interfacial Electrochem*. 1979;101:19–28.
35. Karastogianni S, Girousi S. Sensing in electroanalysis. In: Kalcher K, Metelka R, Svankara I, Vytras K, eds. *Electrochemical Behavior of Triethanolamine at a Carbon Paste Electrode*. Vol 8. Pardubice, Chech Republic: University Press Center; 2013/2014:244–252.
36. Panagoulis D, Pontiki E, Skeva E, et al. Synthesis and pharmacochemical study of new Cu(II) complexes with thiophen-2-yl saturated and α,β-unsaturated carboxylic acids. *J Inorg Biochem*. 2007;101:623–634.
37. Bakardjieva S, Bezdicka P, Grygar T, Vorm P. Reductive dissolution of microparticulate manganese oxides. *J Solid State Electrochem*. 2000;4:306–313.
38. Kokkinos C, Raptis I, Economou A, Speliotis T. Determination of trace Tl(I) by anodic stripping voltammetry on novel disposable microfabricated Bismuth-film sensors. *Electroanalysis*. 2010;22:2359–2365.
39. Saterlay AJ, Foord JS, Compton RG. Sono-cathodic stripping voltammetry of manganese at a polished boron-doped diamond electrode: application to the determination of manganese in instant tea. *Analyst*. 1999;124:1791–1796.